POLITECNICO
MILANO 1863

DIPARTIMENTO DI MECCANICA

mecc

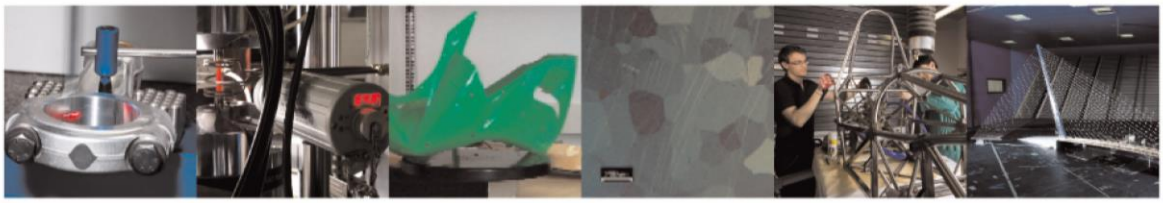

CONTACT AND BENDING FATIGUE BEHAVIOUR OF AUSTEMPERED DUCTILE IRON GEARS

Carlo Gorla, Edoardo Conrado, Francesco Rosa and Franco Concli

This is a post-peer-review, pre-copyedit version of an article Gorla, C., Conrado, E., Rosa, F., Concli, F., Contact and bending fatigue behaviour of austempered ductile iron gears, Proceedings of the Institution of Mechanical Engineers, Part C: Journal of Mechanical Engineering Science, Volume: 232 issue: 6, pages: 998-1008, 2018

The final authenticated version is available online at:
https://doi.org/10.1177/0954406217695846

CONTACT AND BENDING FATIGUE BEHAVIOUR OF AUSTEMPERED DUCTILE IRON GEARS

Carlo Gorla[1], Edoardo Conrado[1], Francesco Rosa[1] and Franco Concli[2]

[1] Dip. Meccanica, Politecnico di Milano, IT
[2] Bonfiglioli BMR, IT - Free University of Bolzano, Faculty of Science and Technology

Abstract

In the present paper a research programme aimed at investigating both the bending and contact fatigue properties of an Austempered Ductile Iron (ADI) applied to gears is presented, in order to determine reliable values of the limits, which take into account the influence of the production process, to be applied in the design of gearboxes. The bending fatigue tests are performed according to the single tooth fatigue (STF) approach and the pitting tests are performed with a back-to-back rig. Metallurgical analysis is performed on the failed specimens, in order to understand the origin and the propagation of the failures and to appreciate the influence of the micro-structure on the performances obtained.

Keywords: AUSTEMPERED DUCTILE IRON, GEARS, BENDING, PITTING, GEARBOX DESIGN

1 Introduction

Small planetary gearboxes used for application in automation can be designed according to different production approaches and using different materials for the casing; nevertheless, due to the strict requirements in terms of backlash and torsional stiffness, low tolerances on gear teeth must be granted.

One typical solution is represented by the adoption of a housing manufactured in cast iron, typical a nodular iron, with the teeth of the internal gear manufactured directly on the casing itself, which combines the advantages of a cost effective production process with the possibility of obtaining complex geometries of the casing.

Generally, in order to meet the requirements of strength for the gear teeth, the manufacturing process requires a heat treating which, due to the distortions must be followed by a finishing step, in order to ensure the required accuracy.

An alternative option is represented by the adoption of Austempered Ductile Iron (ADI), by means of which the requirements of strength and accuracy can be met without the final finishing operation: the teeth can be therefore obtained by broaching and, thank to the low distortion which can be granted by the austempering process, a subsequent finishing process can be avoided.

For all these reasons, ADI represents an appealing solution for manufacturers; nevertheless, even if ADI has been used in the manufacturing of gears since the seventies of the past century, due to the limited experience and data available for such material, the design and rating phases could represent a critical step.

It is recognized that, in order to obtain a reliable estimation of the performances, the material data to be used for the rating of gearboxes according to the existing standards, must be necessarily obtained by test made on gear specimens, both for bending fatigue and contact fatigue limits, as those provided by the standards themselves. In fact, the use of data derived by standard specimens adapted to the gear rating would introduce a lot of uncertainties and hypotheses in the calculation method, with the unavoidable consequence that the performances rated would be only a rough estimation of the reality.

For the specific case of ADI, few data of such type are available in literature and in Standards.

The Standard ISO 17804 [1] provides bending and contact fatigue limits for ausferritic spheroidal

graphite cast irons of different grades, which could be used for design in combination with the curves for Y_{NT} and Z_{NT} factors, which practically define the shape of the *S-N* curve to calculate the fatigue strength at different numbers of cycles, provided by the Standard ISO 6336-5 [2], respectively for bending and pitting. Nevertheless, the ISO standards does not refer in an explicit way to ADI and the curves for different families of cast irons should be considered.

The Information Sheet AGMA 939 [3] provides bending fatigue and pitting limits, together with Y_N and Z_N specifically for ADI.

The analysis of the available data points out that the different existing standards provide:

- Different value of the limits and different dependency from the specific variant of the material and/or from other properties or other post treatment
- Different trends for the shape of the S-N curves
- Some shaded areas of scattering both for the values and for the trend of the S-N curves, and in particular different assumptions concerning the region of the fatigue limit and the existence of the fatigue limit itself.

Additionally, on the basis of the previous experiences of the authors, which have performed and published several tests on gears materials, mainly case hardened and nitriding steels (see, for example, [4], [5] and [6]), it can be stated that the fatigue strength of gears is influenced by many parameters that combined can determine large variations of the effective performances. In particular the fatigue performances are influenced by defects, by the state of the surface, by the local geometry at the tooth root, by the residual stresses determined by the heat treatment and the machining process.

For all this reason, it can be stated that the final performances of gears applied in power transmissions are the sum of a series of factors, including:

- Material
- Manufacturing process of the gear blank
- Cutting and finishing of the gear teeth
- Heat treatment

Since all these elements can never be identical in different applications, from the point of view of design the effective performances of a gearbox can be determined by rating in a reliable way only if it is possible to take into account the specific manufacturing process.

For all this reasons, in the context of the design of an innovative family of low backlash and high torsional stiffness planetary gearboxes for application in automated systems, the performances of which must be granted accurately, the manufacturer has started a research program aimed at the experimental investigation of gear data corresponding to the effective properties of the product.

The test campaign has been performed on gear specimens representative of all the geometrical and technological properties of the real product, including the casting process, the tooth root geometry, the heat treatment, cutting and finishing processes and residual stresses.

Moreover, in the present research program, both the bending and contact fatigue properties have been investigated in order to have consistent data on specimen coming from the same productions lots.

The bending fatigue tests have been performed with the STF (Single Tooth Fatigue) approach (a description of the more common approaches can be found in [7]), in which the gear loads are applied by means of anvils without reproducing the gear meshing with a mating gear. Instead the pitting tests, for which the effective meshing condition must necessarily be reproduced in the test, have been performed by means of an FZG type back-to-back test rig [8].

2 Material

The material investigated in the present research is an ausferritic spheroidal graphite cast iron obtained by means of an austempering heat treatment. The chemical composition of the base material is reported in Table 1. Table 2 lists the mechanical properties of the material measured on machined test pieces cut out from cast samples after the heat treatment process. On the basis of these mechanical properties, the material can be classified, according to [1], as an ADI grade ISO 17804/JS/800-10.

Table 1: Chemical composition (wt%) of the base material.

C	Si	Cu	Ni	Mo	Mn
3.65	2.40	0.65	0.07	0.15	0.20

Table 2: Mechanical properties of the material.

Hardness HBW	R_m $[MPa]$	$R_{p0.2}$ $[MPa]$	A [%
288	830	572	10.

Test performed on machined test pieces cut out from cast sa subjected to the heat treatment process.

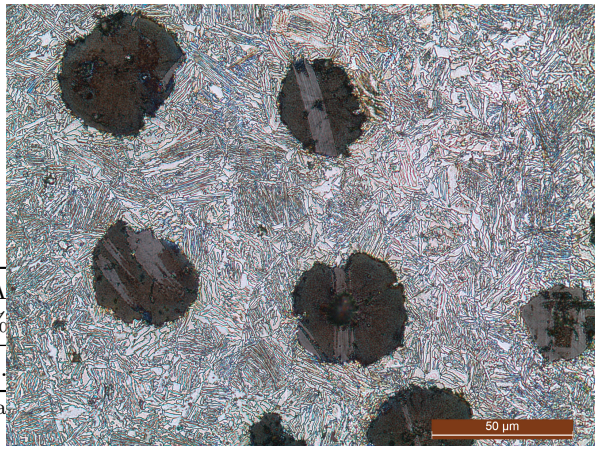

Figure 1: Austempered ductile iron microstructure (Optical micrograph 500x after polishing and 4% nital etching).

The material of gear specimens were inspected prior to testing in order to characterize the material structure obtained from the heat treatment process. A metallographic examination by comparative visual analysis was performed on one tooth of an untested gear specimen. The results showed that the austempered ductile iron had an ausferritic matrix structure (see Figure 1), with a uniform distribution of the graphite nodules of regular or slightly irregular spheroidal shape. Hardness measurements were performed on some teeth of untested gear specimens. The average value of the gear specimen macro-hardness measurements was equal to $308.7 HBW 2.5/187.5$ with a standard deviation of $4.6 HBW 2.5/187.5$. The measured macro-hardness values were consistent with micro-hardness (micro-Vickers) measurements performed on the ausferritc matrix of the material from which an average value of $307.3 HV 0.5$ with a standard deviation of $63.5 HV 0.5$ resulted.

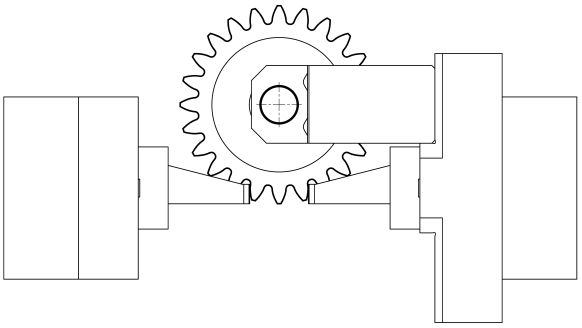

Figure 2: Bending test schematic representation.

3 Bending

The STF fatigue tests have been performed by means of a Schenck mechanical resonance pulsator, capable to apply a maximum load of $60\,kN$. As Figure 2 shows, two teeth of the specimen are loaded at the same position along the profile by means of two anvils which are respectively connected to the fixed and the mobile part of the machine. The specimen is only supported by the two anvils, in order to avoid the static indeterminacy that would be introduced by a supporting pin in the gear blank hole and also in order to allow the immediate removal of the specimen when the tooth brakes, so to avoid potential damages that could be caused by the contact with the mobile anvil which continues to pulsate for some time after the end of the test.

Nevertheless, a pin and a fork connected to the fixed anvil are used in order to grant an accurate symmetric position of the specimen and are removed before the test is started. Since it is necessary to keep always a minimum compressive load on the specimen during the test, the applied load is characterized by a load ratio R (minimum to maximum ratio) of 0.1. This value, on the basis of the experience, is sufficient to avoid undesired displace-

ments of the specimen.

As discussed in [4], by adapting the length of the fixed anvil, the same principle described above can be applied also to perform tests with an asymmetric load condition between the two loaded teeth, either in order to obtain a proper value of the applied load, with respect to the range of loads that can be applied by the machine, or to effectively perform a real "single tooth" test, to avoid having two teeth loaded at the same test stress.

In the present research, the design of the specimen for bending fatigue tests have been performed in order to take into account the properties of the real application, the available tools and the performances of the testing machine.

The aim of the bending test was to determine the fatigue limit through a staircase approach and, taking into account that typical ISO S-N curves assume that the knee is at $3 \cdot 10^6$ cycles, the run-out has been set at 5 million cycles. The staircase procedure has been defined according to Dixon [9].

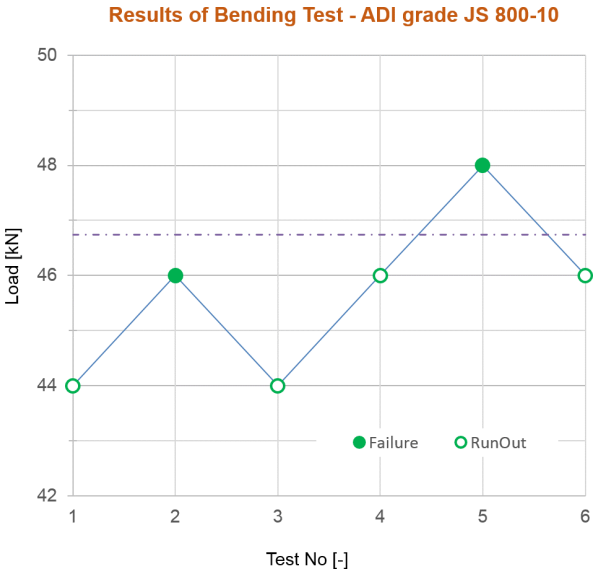

Figure 3: Bending fatigue tests results

3.1 Test gears

The main gear data of the specimens used for the bending fatigue tests are reported in Table 3.

Table 3: STF Gear main data

Description	Symbol	Value
Normal module	m_n	$5\,mm$
Normal pressure angle	α_n	$28\,°$
Tool tip radius coefficient	ρ^*_{fP}	0.375
Tool addendum coefficient	h^*_{fP}	1.296
Tool dedendum coefficient	d^*_{fP}	1.096
Addendum Modification coefficient	x	+0.200
Teeth number	z	36

Table 4: Bending fatigue tests results

Test ID -	MAX Load kN	MIN Load kN	Cycles -
Preliminary Tests (not used)			
0	−3.0	−30.0	RUNOUT
0	−3.4	−34.0	RUNOUT
0	−4.0	−40.0	RUNOUT
0	−4.2	−42.0	RUNOUT
Tests (used to define bending fatigue limit)			
1	−4.4	−44.0	RUNOUT
2	−4.6	−46.0	1′611′316
3	−4.4	−44.0	RUNOUT
4	−4.6	−46.0	RUNOUT
5	−4.8	−48.0	821′414
6	−4.6	−44.0	RUNOUT
Additional Tests (not used)			
0	−5.8	−58.0	238′958
0	−5.4	−54.0	389′605
0	−5.0	−50.0	681′330

3.2 Test results

Figure 3 summarizes the test results listed in Table 4, which includes also additional test points that are not considered in the staircase. Some of them are run-out at low load, which have been obtained before reaching the region of the fatigue limit, and some of them are additional failures obtained in the region of the fatigue strength.

The data have been processed in order to obtain the fatigue limit (X_{50}) with 50 % of probability of

failure by the equation:

$$X_{50} = X_f + K \cdot d \tag{1}$$

where d is the step load step and K is obtained by the table provided by Dixon [9], obtaining:

$$X_{50} = 46 + 0.372 \cdot 2 = 46.7\ kN \tag{2}$$

The stress-load relation has been obtained by applying the procedure of the method B of Standard ISO 6336-3 [10] and according to it the following values of the relevant factors have been determined:

$$Y_F = 6 \cdot \frac{\left(\frac{h_{Fe}}{m_n}\right)}{\left(\frac{s_{Fn}}{m_n}\right)^2} \cdot \frac{\cos\alpha_{Fen}}{cos\alpha_n} = 0.8676 \tag{3}$$

$$Y_s = (1.2 + 0.13 \cdot L) \cdot q_s^{\frac{1}{1.21+2.3/L}} = 2.5615 \tag{4}$$

where

$$s_{Fn} = \frac{s_{Fn}}{2 \cdot \rho_F} \tag{5}$$

$$L = \frac{s_{Fn}}{h_{Fe}} \tag{6}$$

and with the following equation

$$\frac{\sigma_{F0}}{F} = \frac{Y_F \cdot Y_S}{b \cdot m_n} \cdot \cos\alpha_n \tag{7}$$

on the basis of which it results that a load of 1 kN corresponds to 10.44 MPa. The 50 % failure fatigue limit in terms of stress therefore becomes:

$$x_{50} = 487.55\ MPa \tag{8}$$

3.3 Fractographic analysis

The fracture surface of all the specimens where observed by means of a Scanning Electron Microscope (SEM). It is worthy pointing out that the fatigue behavior of the material under consideration, which is obtained by casting, can be influenced at a great extent by the defects, and in particular by the porosity or cavities that could be typical spots of initiation. This consideration is in agreement with the fracture propagation mechanism in ADI described by Lin et al. [14] on the basis of an extensive experimental campaign on rotary bending fatigue.

It must be also pointed out that as explained and demonstrated by testing by Lin et al. [14], who have performed rotating bending fatigue tests on ADI specimens with different heat treatments parameter and different microstructures, that the high cycle fatigue behavior of ADI can be significantly influenced by austempering temperatures and by the size and number of graphite nodules. For this reason, the knowledge of the microstructural properties of the tested specimen provides a necessary basis to check if the properties of components manufactured in the future are consistent with those of the specimens and therefore similar performances are reasonably to be expected.

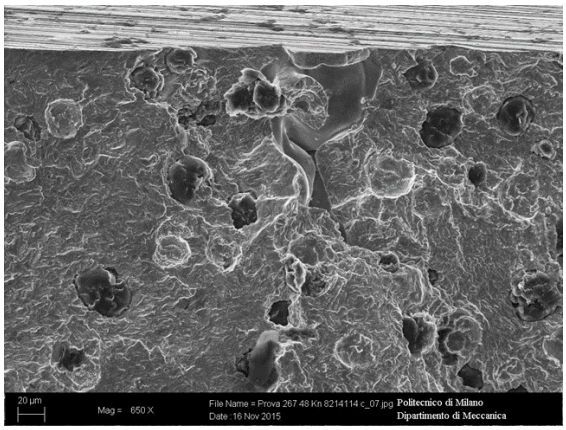

Figure 4: Typical micro-porosity observed on tooth No. 14 of gear No. 1, failed after 821414 cycles at 48 kN.

Generally speaking, on the analysed surfaces, the fracture does not seem to originate from a single point and beach marks have not been observed. It appears that the fractures originate from multiple local defects, like micro porosities or graphite nodules, specially if localized next to the external surface.

Figure 4 and 5 show examples of the surfaces of fracture. The SEM analyses have also confirmed that the maximum size of the micro-porosities was about 20μm, thus confirming that the casting process was producing specimens in accordance with the specifications.

4 Pitting

The objective of the pitting tests performed in the present research was to investigate the fatigue

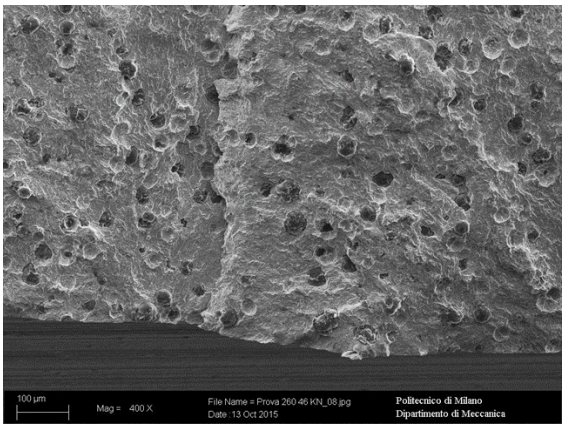

Figure 5: Nodules of graphite next to the external (tooth No. 7 of gear No. 4, failed after 1611316 cycles at 46 kN)

strength region for lives up to 10^7 cycles and, in particular, the region between 10^6 and 10^7 cycles was focused. The specimens were specifically designed for the purpose and the tests were performed on a mechanical recirculating power test bench, installed in the laboratories of the Department of Mechanical Engineering of Politecnico di Milano (Figure 6).

4.1 Test rig

The four-square test rig, as in the typical FZG type configuration, is constituted by two gearboxes, a service gearbox and a test gearbox, connected by two parallel shafts, so obtaining a mechanically closed circuit. On one shaft, the traditional mechanical coupling, which in the original FZG test rig is used to introduce the torque in the system, is here substituted by a rotating hydraulic actuator, by means of which the torque can be applied and varied also during the operation of the rig, thus enabling test at VLA (Variable Load Amplitude). On the other shaft, a torque meter based on strain gauges measures the applied torque. The bench is actuated by an asynchronous motor, controlled by an inverter, which only needs to provide the power losses of the system. The bench is equipped with two independent lubrication circuits, one dedicated to the service gearbox and the hydraulic actuator, and the second for the test gearbox, for which the lubricant properties, the lubrication type and the temperature can be set independently. The centre distance is fixed and equal to 91.5 mm, the maximum torque is 1000 Nm up to a speed of 3000 rpm, with splash or jet lubrication up to 120°C.

4.2 Test gears

The test gear pair, the main data of which are summarized in Table 5, was designed with the aim of promoting the failure by pitting with respect to the other types of damages, like, in particular, micropitting, scuffing and bending fatigue, taking into account of the given centre distance of 91.5mm and of the gear ratio of the service gearbox, that must be the same of the test gears. The gear pair was made of a pinion with 17 teeth and a gear with 18 teeth which, being prime numbers determine the hunting teeth condition. The profile shift of the gears was selected in order to increase the bending strength and to reduce the pitting resistance.

Table 5: Pitting test gears - Main data

Description	Symbol	Unit	Value
Center distance	a	(mm)	91.5
Facewidth	b	(mm)	14
Module	m	(mm)	5
Pressure angle	α	(°)	20
Helix angle	β	(°)	0
Number of teeth			
Pinion	z_1	$(-)$	17
Wheel	z_2	$(-)$	18
Profile shift coefficient			
Pinion	x_1	$(-)$	0.4753
Wheel	x_2	$(-)$	0.4450
Tip diameter			
Pinion	d_{a1}	(mm)	99.509
Wheel	d_{a2}	(mm)	104.206
Tool basic rack profile			
Addendum per unit module	$h^\star_{aP0}$	$(-)$	1.294
Root fillet radius	$\rho^\star_{fP0}$	$(-)$	0.375
Flank Surface Roughness	Ra	(μm)	0.94
Accuracy grade		ISO AG 5	
Heat treatment		Austempering	
Surface Hardness		309 HBW	
Profile modifications		None	

4.3 Test procedure

The load levels were selected in order to investigate the region between 10^6 e 10^7 cycles. In particular, three load levels equal to 200, 240 and 280 Nm were considered and the tests were conducted at

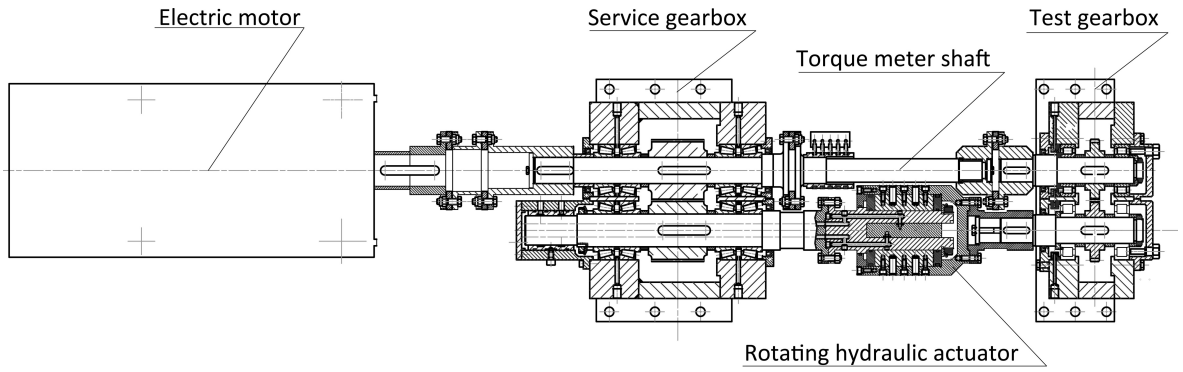

Figure 6: Mechanical recirculating power test rig for tests on gears.

constant load for each of these values. For all the tests the speed of the pinion was 3000 *rpm* and the lubrication was an oil jet "in mesh" at a temperature of $60°C$, with a mineral oil ISO VG 220, with EP additives to increase the safety with respect to scuffing. All the tests were performed up to a pitting damage condition, with the exception of a preliminary test at lower load which has been interrupted at 10^7 cycles. The failure condition, in accordance with [15], has been by convention defined has an extension larger than 4 % of the active surface on a single tooth flank. In order to detect the damage, the tests were regularly interrupted, with regular steps before the damage appearance and successively with closer steps to reach the limit condition.

4.4 Contact stresses

The values of contact stresses, corresponding to a given applied pinion torque, for the pinion and the mating gear, σ_{H1} and σ_{H2}, were calculated according to Standard ISO 6336-2 [16] with the following equations:

$$\sigma_{H1\backslash 2} = Z_{B\backslash D}\sigma_{H0}\sqrt{K_A K_V K_{H\beta} K_{H\alpha}} \qquad (9)$$

where the nominal contact stress at the pitch point, σ_{H0}, is calculated as

$$\sigma_{H0} = Z_\epsilon Z_\beta Z_H Z_E \sqrt{\frac{F_t}{d_1 b}\frac{u+1}{u}} \qquad (10)$$

Table 6 shows the values of contact stresses calculated at the different test loads along with the influencing factors necessary for their calculation. The nomenclature and symbols used, as well as the calculation methods, are those of the Standard ISO 6336-2 [16].

4.5 Test results

The test results are summarized in the diagram of Figure 7, which is in term of contact stresses. Here, the results of each test are represented by the number of cycles to failure (referred to the number of pinion rotation) combined with the test load and the corresponding contact stress at the LPSC (Lowest Point of Single Contact) of the pinion σ_{H1}.

In order to estimate the parameters that identify the median S-N curve, the test results were fitted by means of the method of linear least square in accordance with the Standard ISO 12107 [17], which deals with the statistical analysis of fatigue tests. The trend of the S-N curve, in the range of fatigue lives considered, was assumed linear in a bi-logarithmic diagram according to ISO 6336 and AGMA 939-A07 and described as follows

$$Y = b_0 + b_1 X \qquad (11)$$

where $X = log_{10}(\sigma_{H1})$ and $Y = log_{10}(N_1)$. Parameter b_0 resulted equal to 38.133 and b_1 to -10.353 with a standard deviation equal to 0.1753.

Figure 7 shows the median S-N curve obtained along with the ones corresponding to 10 % and 90 % failure probabilities.

On the same diagram in Figure 7, in order to make a comparison between the test data and the values which can be determined on the basis of the strength data provided by the standards, the limit

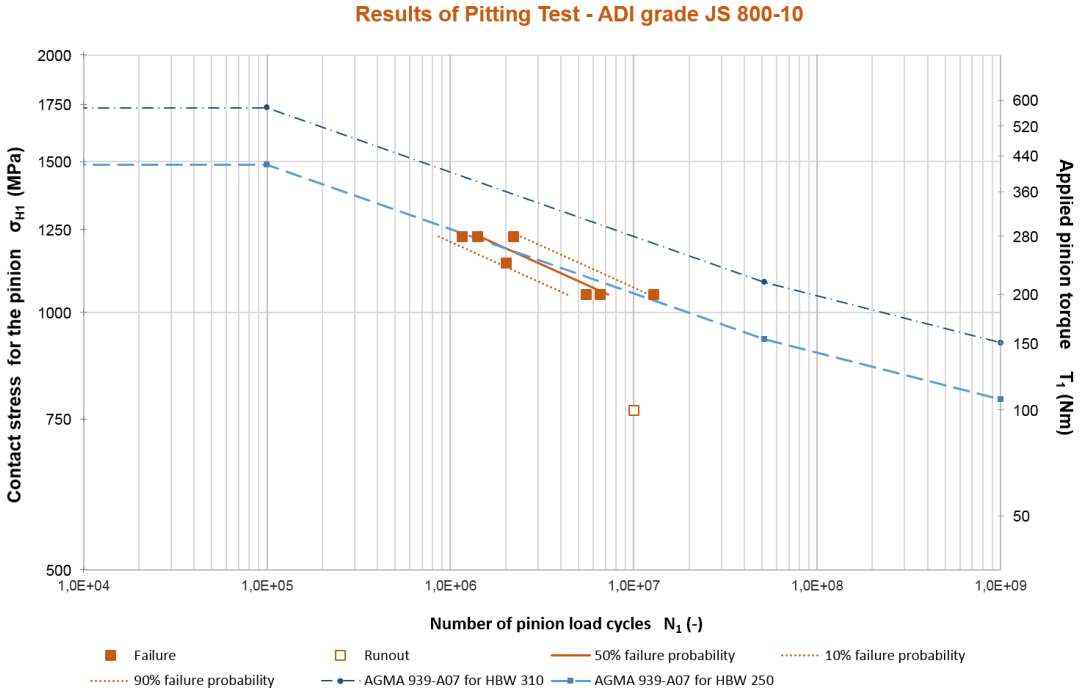

Figure 7: Test results for gears in ADI JS 800-10 compared with limit curves draft according to AGMA 939-A07.

contact stresses of the σ_{HG}, "pitting stress limit", versus the number of cycles is shown. The values were calculated according to ISO 6336-2:2006 as follows:

$$\sigma_{HG} = \sigma_{Lim} \cdot Z_L \cdot Z_V \cdot Z_R \qquad (12)$$

In this equation, since the ISO standard does not provide for this family of materials neither the values of strength nor the factor Z_{NT}, they were obtained by AGMA 939-A07. Table 7 lists the results.

The results depicted in Figure 7 were determined using the nominal hardness values. Even if the measurements of tooth flank hardness resulted in an higher average value (about 309 HBW), the test results were close to the minimum value of the range (corresponding to 250 HBW).

4.6 Evolution of the damage during the tests

In order to monitor the evolution of pitting, visual inspections at least at each million cycles were performed, both on the pinion and on the gear, to appreciate the state of the damage and/or to assess the reaching of the limit. The state of the active flanks, when damaged, was documented by means of pictures.

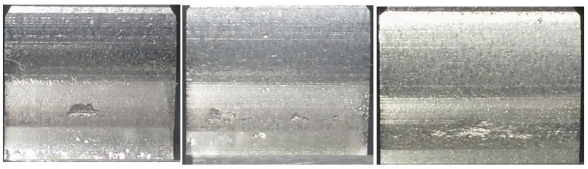

Figure 8: Active flanks of three pinion teeth after 5.0 million cycles at 200 Nm

In all the tests, the failure condition was reached because the limit extension of the damaged surface area was exceeded on one or few teeth of the pinion. For tests at higher torques (240 e 280 Nm), before the last test stage, the pitting damage was found only on the pinion, while, in tests at lower load (200 Nm), the damage occurred also on the teeth of the gear. In this case the damage even occurred on the gear before the pinion, nevertheless

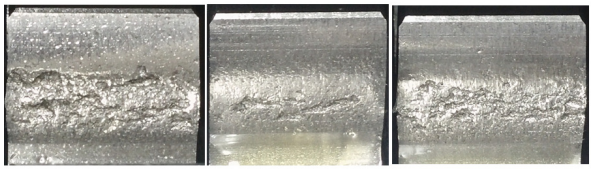

Figure 9: Active flanks of three pinion teeth after 5.5 million cycles at 200 Nm (end of the test).

the damage on the teeth of the gear appeared always in a light way and with a significantly slower evolution. On the contrary, the pitting on the pinion teeth was always of the destructive type. The appearance of small pits on the surface of pinion teeth was in all cases followed by a severe damage that reached the limit condition in a number of cycles lower than 0.5 million. Both on pinion and gear teeth the damage occurred on the dedendum of the active flank, where the damage was promoted by a negative sliding condition. Figure 8 and 9 show an example of damage evolution.

It is worthy to point out that, even though not in a severe form, also a micropitting damage occurred on all the tested gears diffuse on all their teeth. The micropits were first detected by visual inspection with a portable microscope at about one million load cycles during the tests conducted at 280 Nm and 240 Nm, and, during the tests at 200 Nm, at about two million load cycles. At the end of the tests conducted at 200 Nm, the progressive wear of the tooth profile caused by micropitting resulted in a variation of the tooth profile form deviation from iso accuracy grade 5 to 7.

4.7 Contact fatigue mechanism

In order to analyze the contact fatigue damage process, three teeth of a pinion tested at the maximum load level were analyzed ex-situ by means of a SEM. The teeth were sectioned on a transversal plane and, after polishing, the section surfaces were inspected.

The contact fatigue damage on the analyzed teeth, see Figure 10, appeared on the active surface similar to the one typically obtained for case carburized gears in this type of tests, with a diffuse light micropitting damage, concentrated particularly in the dedendum of the tooth, followed, on few teeth, by the formation of macropits. Nevertheless, the form of macropits were more irregular than in case carburized gears, as also observed by Aslantas et al. [18], and they only slightly resemble the typical v-shaped form of spalls observed in case hardened gears. Moreover, micropits appeared with a larger extension and nearly visible to the nacked eyes.

The sections analyzed showed clearly the presence of micropits and surface cracks. The surface breaking cracks were oriented at a shallow angle respect to the contact surface ($10\,^\circ - 30\,^\circ$) and had, as typical in case carburized gears, opposite directions in the dedendum and the addendum of the tooth due to the presence of opposite sliding conditions.

In the performed analysis, the formation of surface-breaking cracks in some cases appeared to be related to the presence of graphite nodules close to the contact surface, but in some others did not: surface-breaking cracks located over and connected to a graphite nodule (see e.g. Figure 11) were found, as previously observed by Magalhaes et al. [19] in experiments with discs at an higher contact pressure level, but also surface-breaking fractures not interacting with graphite nodules were found (Figure 11 and 13).
As observed also in crack propagation tests on ADI [20], the propagation path of cracks appeared to be significantly influenced by the presence of graphite nodules both in the formation of micropits and in the developments of macropits or spalls (Figure 14 and 15).

Few subsurface cracks propagating from and through graphite nodules were found located in the range $20 - 100\ \mu\ m$ below the contact surface as shown for example in Figure 13. The deepest of these cracks were close to the region where the maximum stress level due to hertzian contact pressures can be located using multiaxial fatigue criteria (as proposed in [21] and in [22]). Since macropits or spalls have a typical depth of about $100 - 200\ \mu\ m$, the present analysis suggested that the macropits or spalls can be originated, in this type of materials, by subsurface cracks that, eventually, interact with surface cracks or micropits and develop by means of the propagation of branching cracks interacting with graphite nodules as shown in Figure 15.

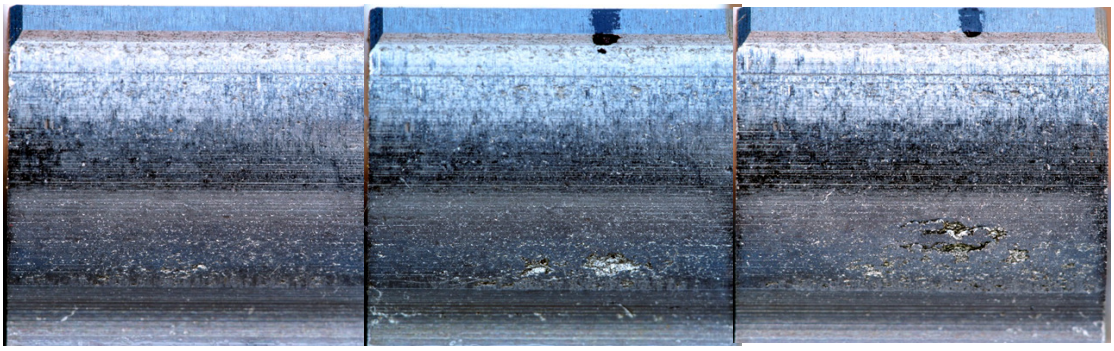

Figure 10: Active flanks of three pinion teeth after 2.2 million cycles at 280 Nm (end of the test). These teeth have subsequently been sectioned and analyzed by SEM. The next figures show the results of this investigation.

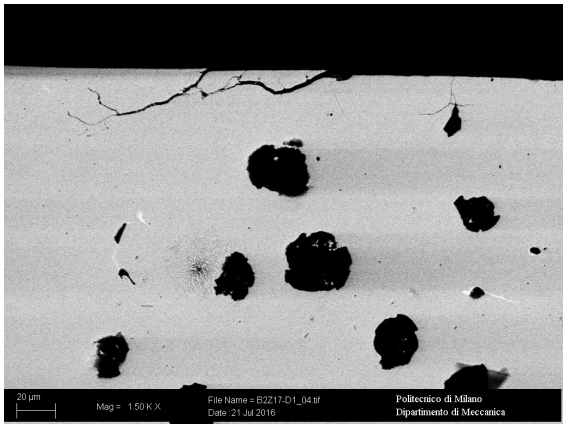

Figure 11: Surface-breaking cracks propagating to form a micropit.

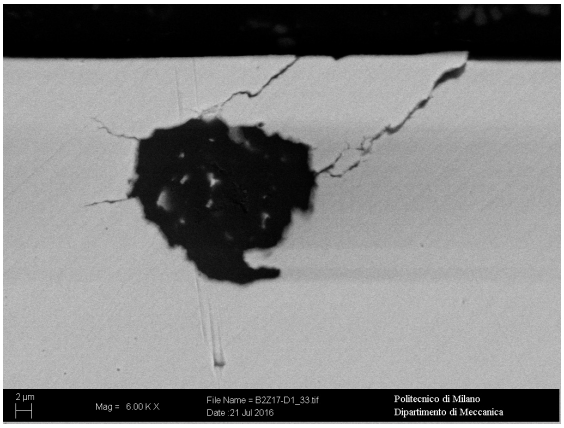

Figure 12: Surface-breaking cracks interacting with a graphite nodule.

5 Conclusions

The limit data for an Austempered Ductile Iron (ADI) to be used in gearbox rating procedure have been determined experimentally, by specifically designing and manufacturing specimens that could be representative of the effective status of the real product, including casting process, machining, heat treatment, local geometry, roughness, residual stresses, etc.

The tests have been performed with the STF (Single Tooth Fatigue) approach for bending and with a recirculating power test bench on meshing gears for pitting.

The data obtained, after the necessary calculation to take into account of the load-stress relation and of the statistical effects, have been compared with those provided by ISO Standard and AGMA Information Sheets, and the comparison has shown that the results obtained are in the ranges provided by these documents. The tests have therefore provided results that on one side are validated by the previous knowledge but that on the other side are more accurate for the specific application.

The limits provided by the tests have been used for the design of an innovative family of low backlash and high torsional stiffness for application in automation, thus providing a more reliable rating of the performances, both at advantage of the manufacturer and of the final customer.

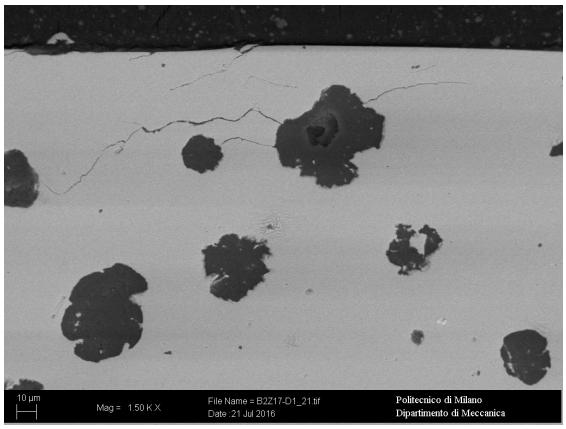

Figure 13: Subsurface crack propagating from and through graphite nodules and some surface cracks.

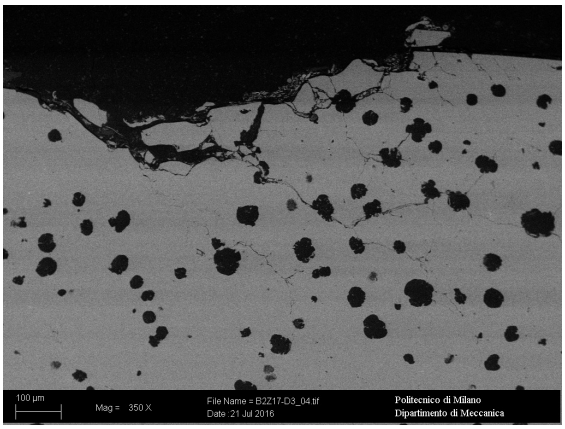

Figure 15: Macropit with propagating branching cracks.

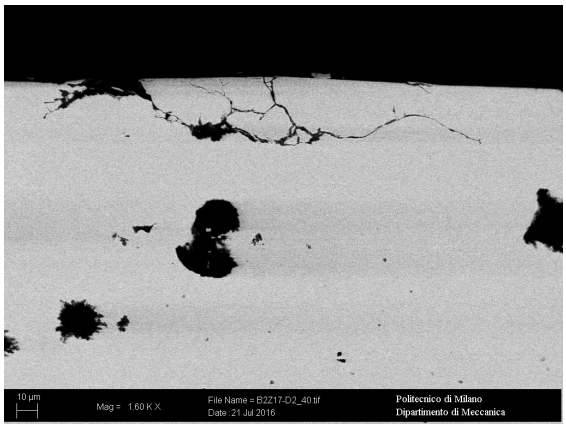

Figure 14: Micropit formation with fractures passing through a graphite nodule.

6 Funding and Conflict of Interest

The research have been funded by Bonfiglioli Mechtronic Research in the context of a public grant received by Provincia Autonoma di Trento.

References

[1] ISO 17804:2005(E) Founding - Ausferritic spheroidal graphite cast irons - Classification.

[2] ISO 6336-5:2003(E) Calculation of load capacity of spur and helical gears - Part 5: Strength and quality of materials.

[3] AGMA 939-A07 - Austempered Ductile Iron for Gears - AGMA Information Sheet.

[4] Gorla, C., Rosa, F., Conrado, E., Albertini, H., Bending and contact fatigue strength of innovative steels for large gears, Proceedings of the Institution of Mechanical Engineers, Part C: Journal of Mechanical Engineering Science, Volume 228, Issue 14, 27 October 2014, Pages 2469-2482

[5] Gorla, C., Rosa, F., Concli, F., Albertini, H., Bending fatigue strength of innovative gear materials for wind turbines gearboxes: Effect of surface coatings, ASME 2012 International Mechanical Engineering Congress and Exposition, IMECE 2012; Houston, TX; United States; 9 November 2012 through 15 November 2012; Volume 7, Issue PARTS A, B, C, D, 2012, Pages 3141-3147

[6] Mariani, U., Molinaro, R., Sartori, S., Gasparini, G., Gorla, C., Improvements in fatigue evaluations of helicopter transmissions, ICAF 2011 Structural Integrity: Influence of Efficiency and Green Imperatives - Proceedings of the 26th Symposium of the International Committee on Aeronautical Fatigue, 2011, Pages 959-969

[7] Gasparini, G., Mariani, U., Gorla, C., Filippini, M., Rosa, F.,Bending fatigue tests of

helicopter case carburized gears: Influence of material, design and manufacturing parameters, American Gear Manufacturers Association Fall Technical Meeting 2008; San Antonio, TX; United States; 12 October 2008 through 14 October 2008; Pages 131-142

[8] DIN 51354 Teil 1 - Prufung von Schmierstoffen FZG Zahnrad Verspannungs Prufmaschine Allgemeine Arbeitsgrundlagen - 1990

[9] Dixon, W., J., The Up-And-Down Method for Small Samples, American Statistical Association Journal, December 1965, pp. 967-978

[10] ISO 6336-3:2006 (E), Calculation of load capacity of spur and helical gears – Part 3: Calculation of tooth bending strength, including Corrigendum 1:2008

[11] Niemann, G., Winter, H., Elementi di Macchine, Vol. 2: Riduttori in generale, riduttori ad ingranaggi, basi, riduttori a ruote dentate cilindriche, Edizioni di scienza e tecnica, Springer, 1983

[12] Rao, S.B., McPherson, D.R., Experimental Characterization of Bending Fatigue Strength in Gear Teeth; Gear Technology, January-February 2003.

[13] Emmert S., G. Schönnenbeck, P. Oster and H. Rettig, Testverfahren zur Untersuchung des Schmierstoffeinflusses auf die Entstehung von Grauflecken bei Zahnrädern, FVA Informationsblatt No. 54/I-IV, July, 1993.5

[14] Lin, C.-K. , Lai, P.-K., Shih, T.-S., Influence of micro-structure on the fatigue properties of austempered ductile irons - I. High-cycle fatigue, Int. J. Fatigue Vol. 18, No. 5. pp. 297-307, 1996

[15] FVA-Information Sheet -Research Project No.2/IV - Pitting Test - 1997.

[16] ISO 6336-2:2006(E) Calculation of load capacity of spur and helical gears - Part 2: Calculation of surface durability (pitting).

[17] ISO 12107:2012(E) Metallic materials - Fatigue testing - Statistical planning and analysis of data.

[18] Aslantas, K., Tasgetiren, S., A study of spur gear pitting formation and life prediction, Wear, 257 (2004) 1167-1175

[19] Magalhaes, L., Seabra, J., Sa, C., Experimental observations of contact fatigue crack mechanisms for austempered ductile iron (ADI) discs, Wear 246 (2000) 134-148.

[20] Greno, G. L., Otegui, J. L., Boeri,R. E., Mechanisms of fatigue crack growth in Austempered Ductile Iron, International Journal of Fatigue 21 (1999) 35-43

[21] Conrado, E., Foletti, S., Gorla, C., Papadopoulos, I.V., Use of multiaxial fatigue criteria and shakedown theorems in thermoelastic rolling sliding contact problems, Wear 270 (2011) 344-354

[22] Conrado, E., Gorla, C., Contact fatigue limits of gears, railway wheels and rails determined by means of multiaxial fatigue criteria, Procedia Engineering 10 (2011) 965-970.

Table 6: Contact stresses and influencing factors at different test loads.

Description	Symbol	Unit		Value	
Pinion Torque	T_1	(Nm)	200	240	280
Contact stress					
Pinion	σ_{H1}	(MPa)	1049	1142	1228
Wheel	σ_{H2}	(MPa)	1039	1131	1216
Pitch contact stress	σ_{H0}	(MPa)	958	1050	1134
Zone Factor	Z_H	(-)		2.154	
Elasticity Factor	Z_E	(-)		170.833	
Contact ratio Factor	Z_ε	(-)		0.939	
Helix angle Factor	Z_β	(-)		1.000	
Single pair pinion	Z_B	(-)		1.034	
Single pair wheel	Z_D	(-)		1.024	
Application Factor	K_A	(-)		1.000	
Dynamic Factor	$K_{V\text{-}B}$	(-)	1.060	1.057	1.054
Face Load Factor	$K_{H\beta\text{-}C}$	(-)	1.056	1.047	1.040
Transv Load Factor	$K_{H\alpha\text{-}C}$	(-)	1.000	1.000	1.000

Calculation according to ISO 6336.

Table 7: Limit contact stresses and influencing factors calculated according to ISO 6336 and AGMA 939-A07.

Name	Symbol	Unit		Value	
Surface hardness		(HBW)	250	280	310
Contact stress limit					
Reference	σ_{HG}	(MPa)	930	1007	1084
Static	σ_{HG}	(MPa)	1582	1699	1817
Allowable stress					
	σ_{Hlim}	(MPa)	989	1062	1136
Zone Factor	Z_L	(-)	1.031	1.027	1.023
Velocity Factor	Z_V	(-)	1.016	1.014	1.012
Roughness factor	Z_R	(-)	0.899	0.910	0.922

Calculation according to ISO 6336 with limit values from AGMA 939-A07.